

Enhanced Broad Band Photodetection through Piezo-Phototronic Effect in CdSe/ZnTe Core/Shell Nanowire Array

Satish C. Rai, Kai Wang, Jiajun Chen, Jason K. Marmon, Manish Bhatt, Sarah Wozny, Yong Zhang, and Weilie Zhou*

The piezo-phototronic effect is of immense importance for improving the performance of optoelectronic nanodevices. This is accomplished by tuning the charge carrier generation, separation, and transport under the influence of the inner piezopotential. In this paper, a broad band photodetector is demonstrated that is based on II-VI binary CdSe/ZnTe core/shell nanowire arrays, in which photodetection is greatly enhanced by the piezo-phototronic effect. The photodetector performance under UV (385 nm), blue (465 nm), and green (520 nm) illumination infers a saturation free response with an intensity variation near two orders of magnitude, where the peak photocurrent (125 μA) is two orders higher at 0.25 kilogram force (kgf) compared to no load (0.71 μA). The resulting (%) responsivity changed by four orders of magnitude. The significant increase in responsivity is believed to arise from: 1) the piezo-phototronic effect induced by a change in the Schottky barrier height at the Ag–ZnTe junction, and in the type-II band alignment at the CdSe–ZnTe interfaces, in conjugation with 2) a small lattice mismatch between the CdSe and ZnTe epitaxial layers, which lead to reduced charge carrier recombination. This work thus extends the piezo-phototronic effect to a group II-VI binary semiconductor heterostructure and demonstrates the importance of the epitaxial interface in a core/shell nanowire photodetector.

1. Introduction

Noncentrosymmetric semiconducting nanostructures have been extensively investigated for mechanical to electrical energy conversion arising from the piezoelectric effect.^[1–4] Wang and Wu have successfully demonstrated that the piezoelectric property

of a semiconductor can be coupled with its optical property to manipulate charge carrier generation/recombination, separation, and transport, coined as piezo-phototronic effect.^[5] This effect has been employed in fabricating a single ZnO micro-/nanowire based UV photodetector with enhanced photosensing performance,^[6] and also in tuning and improving the performance of light emitting devices.^[7–9] It is believed that the inner piezopotential, created by polarization charges, can further increase the carrier lifetime through separation of electrons and holes in different conducting channels provided by the core/shell nanowire geometry.^[10,11] Whereas photo-absorption and carrier transport take place in an orthogonal direction, thereby reducing recombination and scattering losses and, as a result, improving quantum efficiency.^[12–16] This latter strategy was effectively employed to significantly enhance the broad band photodetection response in a single ZnO/CdS core/shell nanowire device.^[17] Regarding the core/shell architecture, three-dimensional (3D) core/shell nanowire array architecture provides additional advantages over single nanowire-based devices owing to their unique features, such as a large surface area, excellent multichannel charge transport, and enhanced light absorption through light trapping and scattering.^[18–21] A 3D ZnO/CdS core/shell, micro-/nanowire-based, UV/visible photodetector was also demonstrated.^[22] Based on these findings, it can be envisaged that 3D core/shell nanowire arrays of semiconducting materials with coupled piezoelectric and photosensitive properties can be effectively utilized to improve photodetector.

As an important II-VI semiconductor, the wurtzite form of CdSe has been widely studied for its application in optoelectronic devices owing to its direct band gap (1.74 eV bulk) and excellent electron transport properties.^[23–25] Previous reports on CdSe nanowire arrays also demonstrated its application in mechanical-to-electrical energy conversion,^[26] and the piezo-phototronic effect was observed in a single CdSe nanowire device.^[27] A more recent study, using a single CdSe/ZnTe core/shell nanowire as a photovoltaic device,^[28] shows that a ZnTe shell can be epitaxially grown on CdSe nanowire, which was attributed to their small lattice mismatch, similar thermal expansion coefficient and type-II band alignment. The

S. C. Rai, Dr. K. Wang, Dr. J. Chen, M. Bhatt, S. Wozny,
Prof. W. Zhou

Advanced Materials Research Institute
University of New Orleans
New Orleans, LA 70148, USA
E-mail: wzhou@uno.edu

J. K. Marmon
Nanoscale Science Ph.D. Program
University of North Carolina
Charlotte, NC 28223, USA

Prof. Y. Zhang
Department of Electrical and Computer
Engineering/Optoelectronic Center
University of North Carolina
Charlotte, NC 28223, USA



DOI: 10.1002/aeml.201400050

promising optical performance from a CdSe/ZnTe core/shell nanowire, as well as, the piezoelectric effect in the CdSe core makes the core/shell architecture an excellent candidate for a piezo-phototronic device. Herein, we report piezo-phototronic effect enhanced UV/Visible, broad band photodetection based on a CdSe/ZnTe core/shell nanowire array with broad spectral detection, high sensitivity, and a fast response.

2. Results and Discussion

2.1. Synthesis and Structural Characterization

CdSe/ZnTe core/shell nanowire arrays were grown with a two-step process as reported previously.^[28] Figure 1a shows a typical low magnification field emission scanning electron microscopy (FESEM) image of a CdSe nanowire array grown on muscovite mica substrate using chemical vapor deposition (CVD). The nanowires are well aligned and are oriented perpendicular to the substrate. They have a length around 5 μm and a diameter around 200 nm. Gold (Au) nanocatalysts are visible at each nanowire end, thereby implying the characteristic vapor-liquid-solid (VLS) growth mechanism. The nanowire aspect ratios (length/diameter) were maintained between 20 and 30 in order to provide the necessary rigidity to withstand incoming ZnTe vapor flux, generated from the subsequent laser ablation process. As shown in Figure 1a, the rational density of nanowires was obtained by carefully controlling the Au catalyst's layer thickness, thus ensuring an optimal ZnTe shell layer coating on the CdSe nanowires with minimized shadow effect. Apparently, the diameter of CdSe/ZnTe core/shell nanowires,

as shown in Figure 1b, increases slightly compared to bare CdSe nanowires in Figure 1a as a result of ZnTe shell layer deposition. A high resolution transmission electron microscopy (HRTEM) image of a single CdSe/ZnTe core/shell nanowire (Figure 1c) reveals good epitaxial growth of the ZnTe shell on the CdSe core nanowire as previously reported.^[28] A lateral energy dispersive X-ray (EDS) line scan across the CdSe/ZnTe core/shell nanowire clearly demonstrates a characteristic core/shell elemental distribution (Figure 1d), further confirming the successful synthesis of a CdSe/ZnTe core/shell nanowire array with an abrupt, nearly lattice-matched interface.

2.2. CdSe/ZnTe Core/Shell Nanowire Array Photodetector

A photodetector was fabricated by positioning a silver (Ag) coated polyester grating on top of an as-synthesized CdSe/ZnTe core/shell nanowire array to achieve optimal bending of the perpendicular core/shell nanowires.^[29] A detailed schematic of device integration and the measurement configuration is shown in Figure 2.

2.2.1. CdSe/ZnTe Core/Shell Nanowire Array Photodetector under Blue Light Illumination

The performance of a CdSe/ZnTe core/shell photodetector under blue illumination ($\lambda = 465 \text{ nm}$) is presented in Figure 3. A typical dark I - V response and under different illumination densities is displayed in Figure 3a, the device photocurrent reached 0.71 μA , which is about a 20-fold improvement compared to the

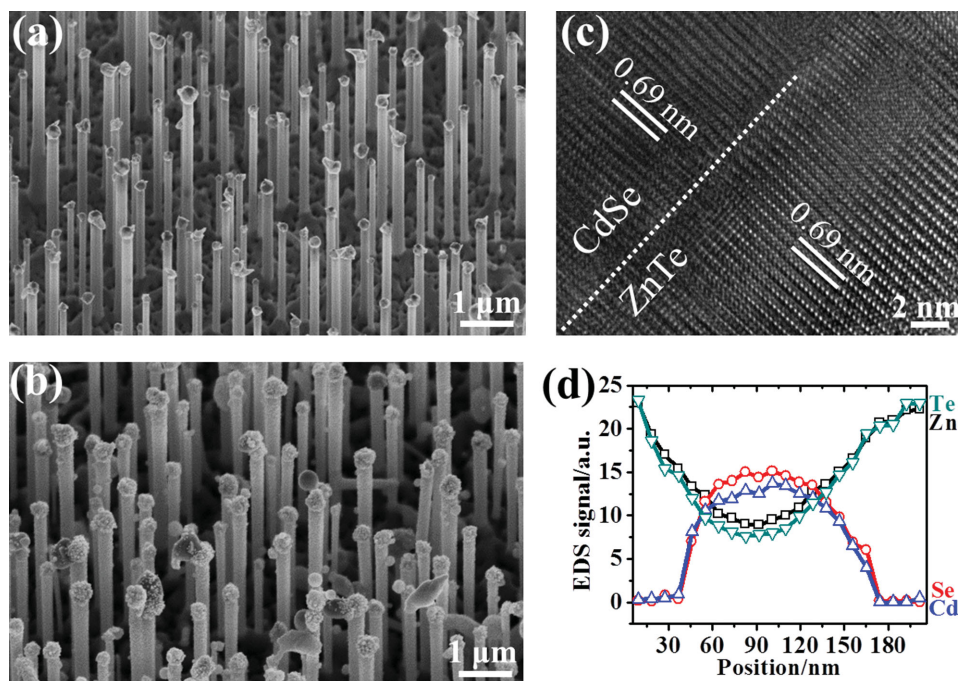


Figure 1. Morphology and structural analysis of CdSe and CdSe/ZnTe core/shell nanowire arrays. a) Low-magnification SEM image of a CdSe nanowire array. b) Low-magnification SEM image of a CdSe/ZnTe core/shell nanowire array. c) HRTEM image of a single CdSe/ZnTe core/shell nanowire. d) A lateral energy dispersive (EDS) line scan across a CdSe/ZnTe core/shell nanowire that demonstrates characteristic core/shell elemental peaks.

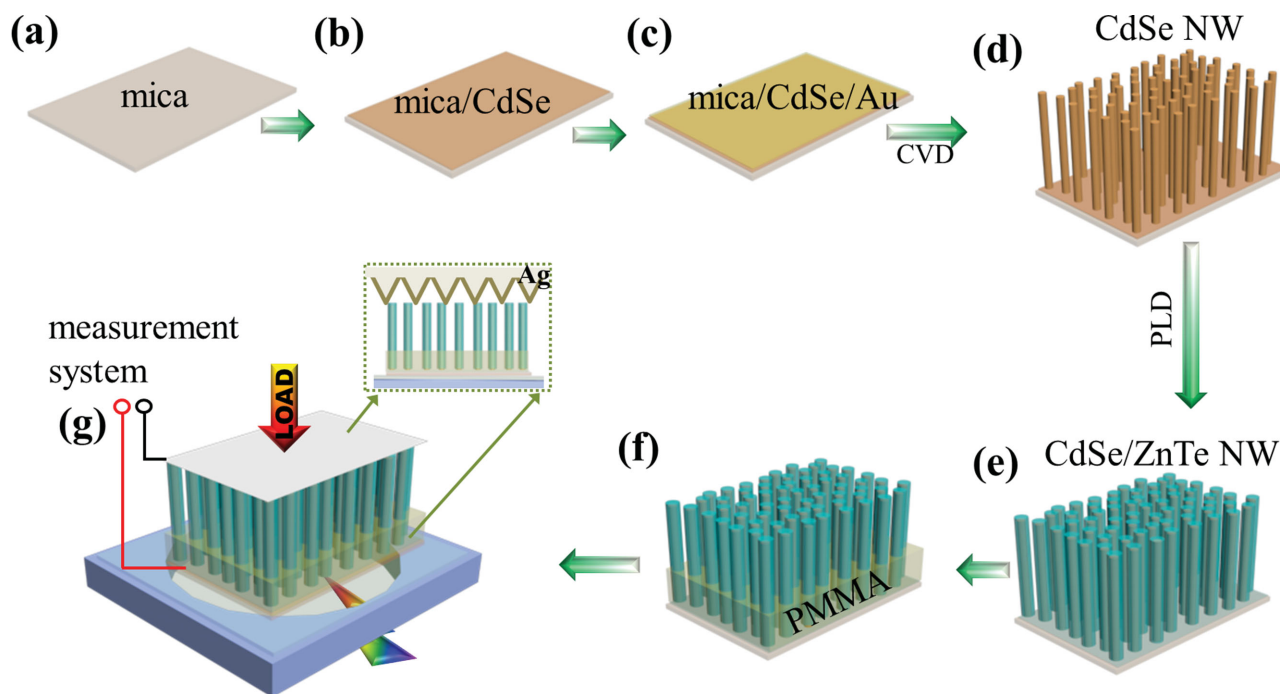


Figure 2. Schematics of the device configuration and measurement set-up. a–c) Preparation of substrate for CdSe nanowire array growth. d) Perpendicular CdSe nanowire array grown by CVD. e) CdSe/ZnTe core/shell nanowire array achieved by pulsed laser ablation of ZnTe shell. f) PMMA layer spin coating. g) Device positioned on PVC board with illumination source underneath and connected to measurement system (inset is a cross-sectional view of the assembled device).

dark current value of $0.03 \mu\text{A}$ with an applied bias of 1.8 V and 3.0 mW cm^{-2} illumination density. The sensitivity of the photodetector, defined as $\frac{I_{\text{light}} - I_{\text{dark}}}{I_{\text{dark}}}$, is found to be $\approx 2.27 \times 10^3\%$ under 3.0 mW cm^{-2} , which is an order of magnitude higher than the best performance of previously reported heterojunction photodetectors, such as P3HT:CdSe^[30] and n-CdSe/p-Cu₂O.^[31] Additionally, there is no obvious saturation under a wide range of illumination densities, which range from 0.3 to 3.0 mW cm^{-2} . This makes the device functional between low to high illumination, which is a critical feature for industrial application. The photocurrent's dependence upon the illumination density is illustrated in Figure 3b. Figure 3c shows the photodetector's on–off current response under blue illumination ($\lambda = 465 \text{ nm}$). The device quickly attains its peak current value, and shows a response speed as high as 0.1 s , which is an order of magnitude higher than a reported ZnTe nanowire-based photodetector.^[32] The improved response stems from increased photo-absorption and electron transport in the CdSe core. It is also observed that the off-current decays slowly, which was attributed to the persistent photocurrent arising from charged surface trap states, and is an effect previously found in other binary semiconductor nanowires.^[33–37]

The performance of a photodetector is also determined by its total responsivity,^[38] as shown in Figure 3d, which is defined as

$$R = \frac{I_{\text{light}} - I_{\text{dark}}}{P_{\text{ill}}}$$

$$P_{\text{ill}} = I_{\text{ill}} \cdot A,$$

where I_{light} and I_{dark} are currents when the photodetector is under illumination and in the dark, respectively. P_{ill} , I_{ill} , and A are the excitation power, illumination density, and the active/illuminated device area, respectively. The calculated responsivity of a CdSe/ZnTe core/shell photodetector under 0.3 mW cm^{-2} of blue excitation ($\lambda = 465$) is 1.6 mA W^{-1} , which is comparable with other heterojunction photodetectors.^[39–41] The decrease in responsivity at higher illumination densities can be attributed to hole-trapping saturation and a transparent Schottky barrier at higher illumination densities.^[6–27]

2.2.2. CdSe/ZnTe Core/Shell Nanowire Array Photodetector under Green and UV Light Illumination

Similar I – V measurements were also performed under green ($\lambda = 520 \text{ nm}$, Figure S1, Supporting Information) and UV illumination ($\lambda = 385 \text{ nm}$, Figure S2, Supporting Information) to investigate the wide spectral responses. The detailed measurements are summarized in Figures S1 and S2, Supporting Information. The measurements under green and UV illumination show an increase in absolute current from 0.03 to $0.18 \mu\text{A}$ (3.24 mW cm^{-2} , 1.8 V bias) and $0.13 \mu\text{A}$ (1.32 mW cm^{-2} , 1.8 V bias), respectively. The significant increase in absolute current (an order of magnitude under blue, a 6-fold increase under green, and more than a 4-fold increase under UV) can be attributed to the epitaxial interface in a CdSe/ZnTe core/shell nanowire array, which leads to significantly reduced recombination and scattering losses. Additionally, it can be seen that the response speed of the device is well preserved (0.1 s) as observed under blue light illumination, which indicates that

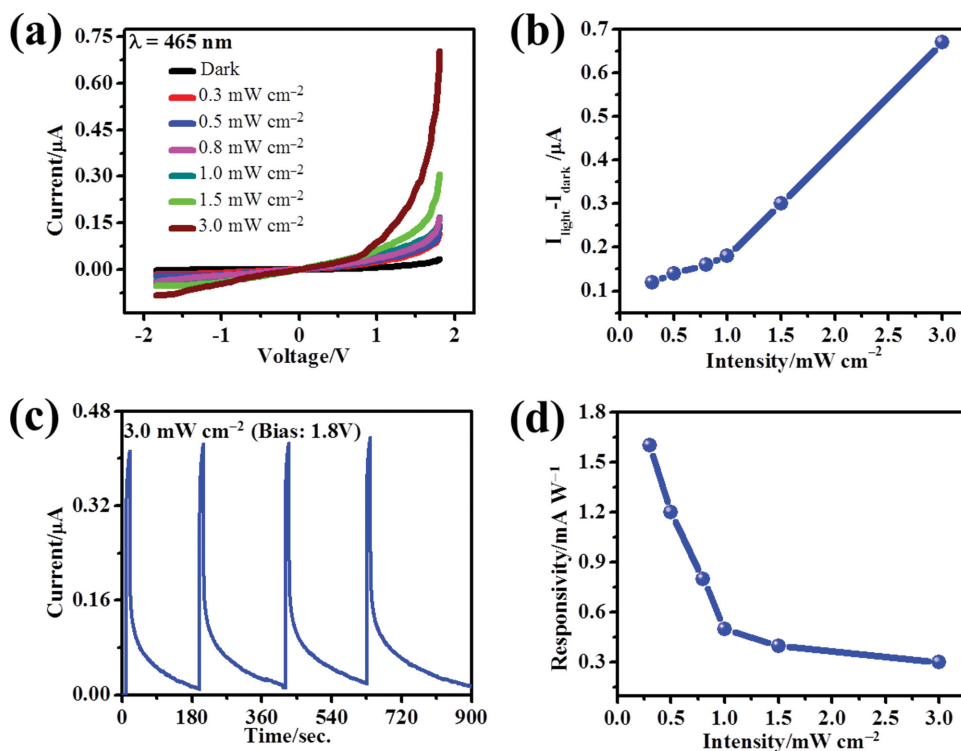


Figure 3. a) I - V measurements of a CdSe/ZnTe core/shell nanowire array device under blue (465 nm) light illumination at variable intensities. b) Absolute current of the device with respect to intensity. c) On-off response of the device at a bias of 1.8 V and under blue illumination. d) Photon responsivity of the device relative to the intensity density of the blue (465 nm) excitation source and bias voltage of 1.8 V.

the CdSe/ZnTe core/shell nanowire array photodetector has a fast and saturation free response under a wide optical range from 385 to 520 nm and illumination densities, e.g., from 0.04 ($\lambda = 385 \text{ nm}$) to 3.24 mW cm^{-2} ($\lambda = 520 \text{ nm}$).

2.3. Piezo-Phototronic Effect in CdSe/ZnTe Core/Shell Nanowire Array Photodetector

To further investigate the piezo-phototronic effect in the CdSe/ZnTe core/shell nanowire photodetector's performance, the device was subjected to compressive loads ranging from 0.05 to 0.30 kgf under blue, green, and UV illumination. **Figure 4a** displays the device I - V measurements under dark blue ($\lambda = 465 \text{ nm}$), green ($\lambda = 520 \text{ nm}$), and UV ($\lambda = 385 \text{ nm}$) illumination without applied loads where current increases with increasing excitation frequency. **Figure 4b** represents the I - V measurements at different loads, e.g., from 0 to 0.3 kgf under blue illumination, and the observed peak current increases from 0.71 μA without load to its maximum of 125 μA at 0.25 kgf load, where a significant two orders of magnitude change can be observed. To investigate the performance of the device under a wide spectral range, similar I - V measurements were performed under green and UV light illumination with identical compressive loads (as the blue excitation source), which are shown in **Figure 4c,d**. The photocurrent reached its maximum value of 83 μA (**Figure 4c**) and 51 μA (**Figure 4d**) at 0.25 kgf compared to no load values of 0.18 and 0.13 μA (**Figure 4a**) for green and UV illumination, respectively. Generally, a sequential

increment in photocurrent with increasing compressive loads from 0.05 to 0.25 kgf can also be seen. **Figure 4e** is the variation of peak photocurrents relative to different compressive loads from 0.05 to 0.30 kgf, representing an increasing tendency of the photocurrent until 0.25 kgf. However, it was found that the photocurrents could not be further enhanced when compressive loads are over 0.25 kgf, as shown; photocurrents decreased once the load is 0.3 kgf. The I - V measurements were repeated for several cycles and showed reproducible results and steady performance. Therefore, structural degradation of the nanowire array as a source of the photocurrent decrease can be ruled out. The reduced photocurrent is similar to the previously reported behavior of a single CdSe nanowire,^[22] and can be explained by a theoretical model based on band bending at the CdSe/ZnTe interface under the influence of the piezopotential, which will be discussed subsequently. The (%) change in responsivity ($\Delta R = (R_{\text{Load}} - R_0) / R_0 \times 100$) of the CdSe/ZnTe core/shell photodetector at compressive loads of 0.05 to 0.3 kgf is shown in **Figure 4f** as well. The calculated (%) change in responsivity between illuminated samples with an applied load of 0.25 kgf and without an external load and under 1.8 V bias results in a change of four orders of magnitude. The variation in responsivity is remarkably high for this 3D, II-VI type-II core/shell nanowire array, which makes it an ideal candidate for a piezo-phototronic effect enhanced photodetector.

The improved photodetector performance under compressive load can be explained by a theoretical model based on the relative band alignment and its modification under the influence of piezopotential at the Ag-ZnTe and type-II, ZnTe/CdSe

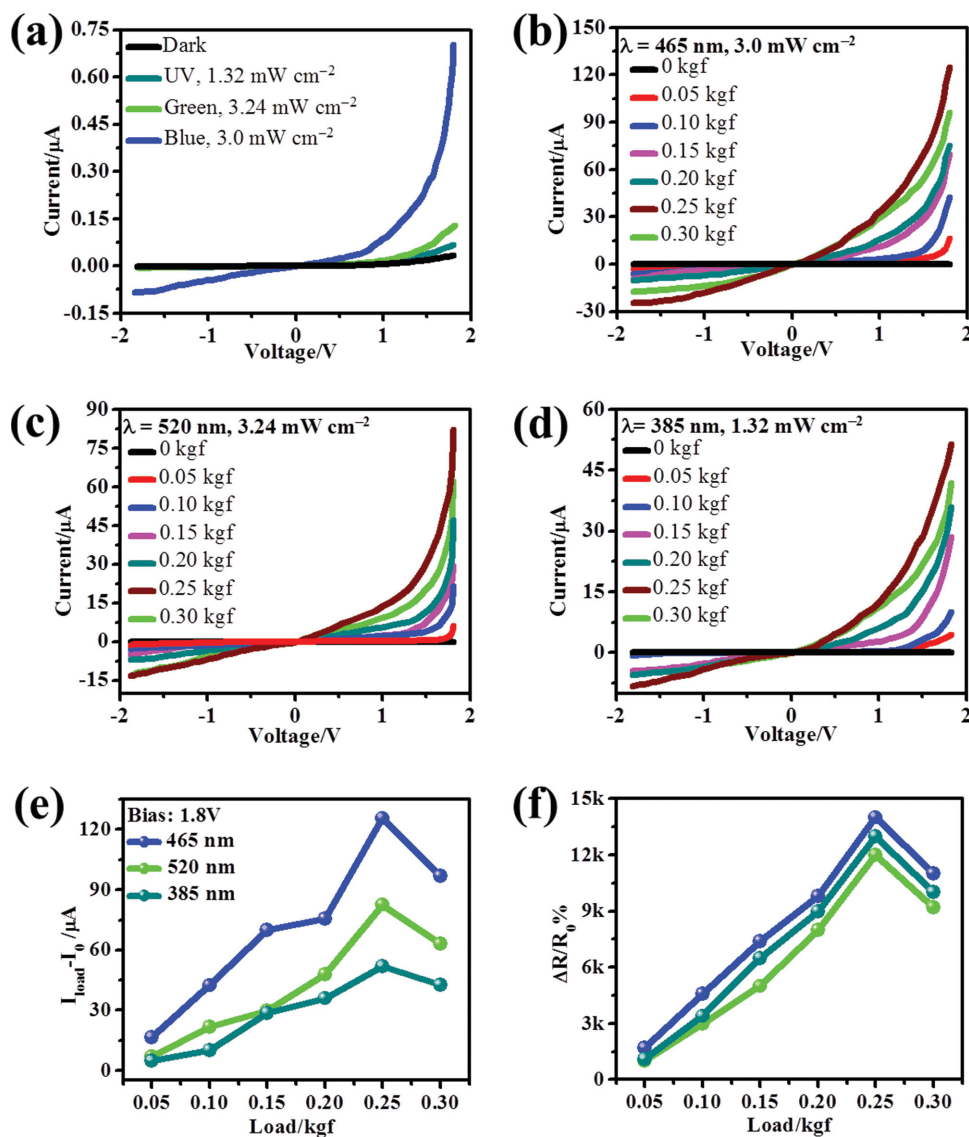


Figure 4. a) I - V characteristic of CdSe/ZnTe core/shell nanowire array device under blue, green, and UV illumination. b-d) A typical I - V for a CdSe/ZnTe core/shell array device under different compressive loads and blue, green, and UV illumination, respectively. e) Absolute current of the device relative to compressive load under blue, green, and UV illumination. f) Change in responsivity of the device subjected to load differences and constant illumination, where R_0 is the responsivity at zero load.

interfaces. As previously reported,^[26] a wurtzitic CdSe nanowire undergoing lateral bending generates positive and negative piezopotentials at the stretched (tensile) and compressed sides, respectively, of the nanowire surface (Figure S3, Supporting Information). This localized piezopotential then modifies the local Schottky barrier height at the Ag-ZnTe and ZnTe-CdSe interfaces, which controls the charge carrier transport and separation at the interface through the piezo-phototronic effect. At equilibrium conditions, it is assumed that no net charge transfer takes place at the CdSe/ZnTe interface due to the staggered band alignment resulting from ZnTe's low-lying Fermi level, and a high electron transport barrier going from CdSe to ZnTe. When a Ag metal electrode is brought in contact with the ZnTe surface, a net diffusion current flows from ZnTe to the metal side resulting in ZnTe's Fermi level moving to lower

energy; this also results into a lowering of the CdSe Fermi level (Figure 5a).^[42,43] Once equilibrium is established, the majority diffusion current is retarded due to Schottky barrier created at the Ag-ZnTe interface. However, this barrier height can be tuned either by applying an external voltage or by modifying the inner piezopotential created in the noncentrosymmetric crystal structure under mechanical deformation, e.g., applying a load. Upon illumination, the photogenerated electron-hole pairs momentarily shift the Fermi level slightly upwards for the thinner ($\approx 20 \text{ nm}$) ZnTe shell since ZnTe has a weak thickness-limited photo-absorption compared to the thicker CdSe core, where moderate Fermi level lowering takes place due to greater absorption in the thicker ($\approx 200 \text{ nm}$), CdSe core (Figure 5b). This Fermi level redistribution gives rise to photocurrent and, at fixed excitation wavelength, increases with increasing

illumination density as observed in illumination density dependent I - V measurements (Figure 3a and Figures S2 and S3a, Supporting Information). When the nanowires are bent under an external load, the appearance of a positive piezopotential at the tensile surface reduces the Schottky barrier height (Figure 5c) at the Ag-ZnTe interface, which leads to increased minority carrier diffusion, electrons from ZnTe and holes from CdSe, flow through the interface. The magnitude of the piezopotential is dependent on the degree of mechanical deformation, therefore higher current flows at increased compressive loads.^[44] However, when the compressive strain is higher than a threshold value, which is 0.25 kgf in our system, it can raise the valence band edge of CdSe above ZnTe's valence band edge, as shown in Figure 5d, creating hole trapping states that lead to a decrease in the total current, as observed for 0.3 kgf load. The piezopotential lowering of the barrier height at the Ag-ZnTe interface and photo-excitation causing relative Fermi level redistribution create, in conjunction, a favorable situation for higher charge carrier injection between the Ag-ZnTe and ZnTe/CdSe interface (Figure 5d) is created. It should be noted that unidirectional charge carrier injection, a combined effect of the piezopotential and photo-excitation, is greatly enhanced owing to the epitaxial nature of the CdSe/ZnTe interface, thereby resulting in higher peak current and a remarkably high responsivity change under simultaneous employment of load and illumination.

3. Conclusion

In summary, a broad band photodetector based on a type-II, epitaxially grown CdSe/ZnTe heterojunction core/shell nanowire array has been successfully integrated. The epitaxial nature of the interface plays an important role as manifested by a high responsivity and significant sensitivity even at low illumination densities. The device performance is greatly enhanced by

simultaneous application of compressive load and illumination owing to the piezo-phototronic effect. Two orders of magnitude change in the absolute current along with four orders of magnitude change in responsivity has been achieved, which is the highest increment observed so far. This investigation demonstrates the enhanced piezo-phototronic effect in a group II-VI, heterojunction, core/shell nanowire array fabricated as a photodetector.

4. Experimental Section

Synthesis of Vertically Aligned CdSe and CdSe/ZnTe Core/Shell Nanowire Array: The vertically aligned CdSe nanowire array was grown on muscovite mica substrate by chemical vapor deposition.^[45] Briefly, freshly cleaved muscovite mica (Pelco Mica Sheets, grade V5) substrate was transferred to electron beam evaporation system (K. J. Lesker, PVD75) for the deposition of a 100 nm textured CdSe film. The as deposited substrate was then coated with a 3 nm gold layer by DC sputtering (Cressington coating system, 308R), and which serves as a catalyst for the nanowire array growth. The substrate was further loaded in a 1 in. split zone tube furnace (Lindberg Blue M) for the growth of a CdSe nanowire array by thermal evaporation of CdSe powder (Alfa Aesar, 99.999% purity, metals basis) at 750 °C under 200 sccm Ar/H₂ flow. The as-synthesized CdSe nanowire array was transferred to a home-built, pulsed-laser deposition system. The system was pumped down to 30 mTorr and heated up to 350 °C before starting ablation with a Nd:YAG laser (LOTIS-TII, LS2147), which was set to 30 mJ cm⁻² at a repetition rate of 5 Hz and a wavelength of 1064 nm. The ZnTe target was prepared by cold pressing ZnTe powder (Alfa Aesar, 99.95% purity, trace metals basis) that was used as an ablation source. The deposition was performed for 15 min following by natural cooling to room temperature. Detailed information about the synthesis, morphology, structural, and optical characterization was reported previously.^[28]

Device Fabrication: An as-synthesized CdSe/ZnTe core/shell nanowires array was then coated by a thin layer of PMMA ($\approx 2 \mu\text{m}$) to avoid a possible short circuit. A polyester plate with a grating containing 12700 lines per inch (Edmund Optics) (see the inset of Figure 2) was sputter coated with a 100 nm thin Ag layer that functions as a top electrode. The top electrode and CdSe film on mica substrate were connected by Cu

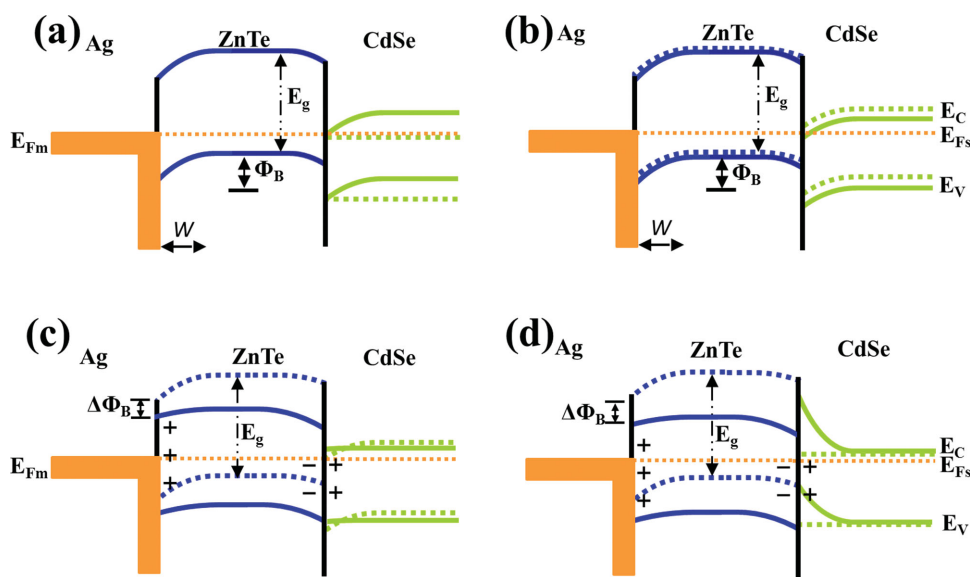


Figure 5. Schematic band alignment of the Ag/ZnTe/CdSe structure. a) At equilibrium. b) Under illumination only. c) Under simultaneous application of compressive load and illumination. d) Under a compressive load of more than 0.25 kgf.

leads using silver paste, respectively, for the electrical measurements. A typical device photograph is shown in Figure S4, Supporting Information, with dimensional details displaying the area of device $\approx 15 \text{ mm}^2$. A UV/visible absorption spectrum (Figure S5, Supporting Information) was collected on bare muscovite mica substrate, mica/CdSe film, and mica/CdSe film/CdSe/ZnTe core/shell nanowire array. No absorption was observed for bare mica between 350 and 800 nm wavelengths, and the absorption for mica/CdSe film is significantly lower than that of core/shell nanowire array, which confirms that absorption mainly takes place in the core/shell nanowire array.

Electrical Measurements: The electrical measurements were carried out with the help of low noise current pre-amplifier (SR-570), and a source meter (Keithley 2401) coupled with computer interface.

Supporting Information

Supporting Information is available from the Wiley Online Library or from the author.

Acknowledgements

S.C.R. and K.W. contributed equally to this work. This research was supported by the DARPA Grant No. HR0011-07-1-0032 and research grants from Louisiana Board of Regents Contract Nos. LEQSF (2008-11)-RD-B-10 and LEQSF (2011-13)-RD-B-08.

Received: December 10, 2014

Revised: January 9, 2015

Published online:

- [1] Z. L. Wang, J. Song, *Science* **2006**, *312*, 242.
- [2] Y. F. Lin, J. Song, Y. Ding, S. Y. Lu, Z. L. Wang, *Appl. Phys. Lett.* **2008**, *92*, 022105.
- [3] T. C. Hou, Y. Yang, Z. H. Lin, Y. Ding, C. Park, K. C. Pradel, L. J. Chen, Z. L. Wang, *Nano Energy* **2013**, *2*, 387.
- [4] M. Minary-Jolandan, R. A. Bernal, I. Kuljanishvili, V. Parpoil, H. D. Espinosa, *Nano Lett.* **2011**, *12*, 970.
- [5] Z. L. Wang, W. Wu, *Nat. Sci. Rev.* **2014**, *1*, 62.
- [6] Q. Yang, X. Guo, W. Wang, Y. Zhang, S. Xu, D. H. Lien, Z. L. Wang, *ACS Nano* **2010**, *4*, 6285.
- [7] Y. Zhang, G. Gao, H. L. W. Chan, J. Dai, Y. Wang, J. Hao, *Adv. Mater.* **2012**, *24*, 1729.
- [8] C. Pan, L. Dong, G. Zhu, S. Niu, R. Yu, Q. Yang, Y. Liu, Z. L. Wang, *Nat. Photon.* **2013**, *7*, 752.
- [9] G. Bai, M.-K. Tsang, J. Hao, *Adv. Opt. Mater.* **2014**, DOI: 10.1002/adom.201400375.
- [10] F. Boxberg, N. Søndergaard, H. Q. Xu, *Nano Lett.* **2010**, *10*, 1108.
- [11] C. Pan, S. Niu, Y. Ding, L. Dong, R. Yu, Y. Liu, G. Zhu, Z. L. Wang, *Nano Lett.* **2012**, *12*, 3302.
- [12] Y. Zhang, Wang, A. Mascarenhas, *Nano Lett.* **2007**, *7*, 1264.
- [13] J. Schrier, D. O. Demchenko, L.-W. Wang, A. P. Alivisatos, *Nano Lett.* **2007**, *7*, 2377.
- [14] K. Wang, J. Chen, W. Zhou, Y. Zhang, Y. Yan, J. Pern, A. Mascarenhas, *Adv. Mater.* **2008**, *20*, 3248.
- [15] K. Wang, J. J. Chen, Z. M. Zeng, J. Tarr, W. L. Zhou, Y. Zhang, Y. F. Yan, C. S. Jiang, J. Pern, A. Mascarenhas, *App. Phys. Lett.* **2010**, *96*, 123105.
- [16] Z. Wu, Y. Zhang, J. Zheng, X. Lin, X. Chen, B. Huang, H. Wang, K. Huang, S. Li, J. Kang, *J. Mater. Chem.* **2011**, *21*, 6020.
- [17] F. Zhang, Y. Ding, Y. Zhang, X. Zhang, Z. L. Wang, *ACS Nano* **2012**, *6*, 9229.
- [18] B. Tian, T. J. Kempa, C. M. Lieber, *Chem. Soc. Rev.* **2009**, *38*, 16.
- [19] M. Law, L. E. Greene, J. C. Johnson, R. Saykally, P. Yang, *Nat. Mater.* **2005**, *4*, 455.
- [20] J. Wallentin, N. Anttu, D. Asoli, M. Huffman, I. Åberg, M. H. Magnusson, G. Siefert, P. Fuss-Kailuweit, F. Dimroth, B. Witzigmann, H. Q. Xu, L. Samuelson, K. Deppert, M. T. Borgström, *Science* **2013**, *339*, 1057.
- [21] M. Yao, N. Huang, S. Cong, C.-Y. Chi, M. A. Seyedi, Y.-T. Lin, Y. Cao, M. L. Povinelli, P. D. Dapkus, C. Zhou, *Nano Lett.* **2014**, *14*, 3293.
- [22] F. Zhang, S. Niu, W. Guo, G. Zhu, Y. Liu, X. Zhang, Z. L. Wang, *ACS Nano* **2013**, *7*, 4537.
- [23] Y. Jiang, W. J. Zhang, J. S. Jie, X. M. Meng, X. Fan, S. T. Lee, *Adv. Funct. Mater.* **2007**, *17*, 1795.
- [24] Y. Yu, P. V. Kamat, M. Kuno, *Adv. Funct. Mater.* **2010**, *20*, 1464.
- [25] L. Zhang, E. Shi, Z. Li, P. Li, Y. Jia, C. Ji, J. Wei, K. Wang, H. Zhu, D. Wu, A. Cao, *Phys. Chem. Chem. Phys.* **2012**, *14*, 3583.
- [26] Y. S. Zhou, K. Wang, W. Han, S. C. Rai, Y. Zhang, Y. Ding, C. Pan, F. Zhang, W. Zhou, Z. L. Wang, *ACS Nano* **2012**, *6*, 6478.
- [27] L. Dong, S. Niu, C. Pan, R. Yu, Y. Zhang, Z. L. Wang, *Adv. Mater.* **2012**, *24*, 5470.
- [28] K. Wang, S. C. Rai, J. Marmon, J. Chen, K. Yao, S. Wozny, B. Cao, Y. Yan, Y. Zhang, W. Zhou, *Nanoscale* **2014**, *6*, 3679.
- [29] X. Wang, J. Song, J. Liu, Z. L. Wang, *Science* **2007**, *316*, 102.
- [30] X. Wang, W. Song, B. Liu, G. Chen, D. Chen, C. Zhou, G. Shen, *Adv. Funct. Mater.* **2013**, *23*, 1202.
- [31] J. Debgupta, R. Devarapalli, S. Rahman, M. V. Shelke, V. K. Pillai, *Nanoscale* **2014**, *6*, 9148.
- [32] Y. L. Cao, Z. T. Liu, L. M. Chen, Y. B. Tang, L. B. Luo, J. S. Jie, W. J. Zhang, S. T. Lee, C. S. Lee, *Opt. Express* **2011**, *19*, 6100.
- [33] O. Katz, G. Bahir, J. Salzman, *Appl. Phys. Lett.* **2004**, *84*, 4092.
- [34] C. Soci, A. Zhang, B. Xiang, S. A. Dayeh, D. P. R. Aplin, J. Park, X. Y. Bao, Y. H. Lo, D. Wang, *Nano Lett.* **2007**, *7*, 1003.
- [35] O. Demichel, M. Heiss, J. Bleuse, H. Mariette, A. Fontcuberta i Morral, *Appl. Phys. Lett.* **2010**, *97*, 201907.
- [36] E. M. Gallo, G. Chen, M. Currie, T. McGuckin, P. Prete, N. Lovergine, B. Nabet, J. E. Spanier, *Appl. Phys. Lett.* **2011**, *98*, 241113.
- [37] J. K. Marmon, S. C. Rai, K. Wang, W. Zhou, Y. Zhang, unpublished.
- [38] Y. Liu, Q. Yang, Y. Zhang, Z. Yang, Z. L. Wang, *Adv. Mater.* **2012**, *24*, 1410.
- [39] H. Zhu, C. X. Shan, B. Yao, B. H. Li, J. Y. Zhang, D. X. Zhao, D. Z. Shen, X. W. Fan, *J. Phys. Chem. C* **2008**, *112*, 20546.
- [40] P.-N. Ni, C.-X. Shan, S.-P. Wang, X.-Y. Liu, D.-Z. Shen, *J. Phys. Chem. C* **2013**, *1*, 4445.
- [41] L. Qin, D. Shao, C. Shing, S. Sawyer, *Appl. Phys. Lett.* **2013**, *102*, 071106.
- [42] X. Feng, Y. Zhang, Z. Wang, *Sci. China Technol. Sci.* **2013**, *56*, 2615.
- [43] W. Wu, C. Pan, Y. Zhang, X. Wen, Z. L. Wang, *Nano Today* **2013**, *8*, 619.
- [44] Y. Gao, Z. L. Wang, *Nano Lett.* **2009**, *9*, 1103.
- [45] M. I. B. Utama, Z. Peng, R. Chen, B. Peng, X. Xu, Y. Dong, L. M. Wong, S. Wang, H. Sun, Q. Xiong, *Nano Lett.* **2010**, *11*, 3051.